Earth and Planetary Science Letters 405 (2014) 274–280

Contents lists available at ScienceDirect

Earth and Planetary Science Letters

www.elsevier.com/locate/epsl

Optimizing multi-station earthquake template matching through re-examination of the Youngstown, Ohio, sequence

Robert J. Skoumal *[,1], Michael R. Brudzinski [2], Brian S. Currie [2], Jonathan Levy [2]

Miami University, Department of Geology, 114 Shideler Hall, Oxford, OH 45056, United States

ARTICLE INFO

Article history:
Received 14 May 2014
Received in revised form 27 August 2014
Accepted 31 August 2014
Available online 20 September 2014
Editor: P. Shearer

Keywords:
induced seismicity
wastewater injection
template matching

ABSTRACT

A series of earthquakes in 2011 near Youngstown, OH, has been a focal point for discussions of seismicity induced by a nearby wastewater disposal well. Utilizing an efficient waveform template matching procedure, the optimal correlation template to study the Youngstown sequence was identified by varying parameters such as the stations utilized, frequency passband, and seismogram length. A catalog composed of 566 events was identified between January 2011 and February 2014. Double-difference relocation refines seismicity to a ~800 m linear streak from the Northstar 1 injection well to the WSW along the same strike as the fault plane of the largest event. Calculated Gutenberg–Richter b-values are consistent with trends observed in other regions with seismicity induced by fluid injection.

1. Introduction

Beginning in March 2011, a series of 10 small (M ~ 2), shallow (~3 km depth) earthquakes were recorded and reported by the Ohio Department of Natural Resources (ODNR) in northeastern Ohio (Fig. 1). The proximity of the events to the recently activated Northstar 1 wastewater disposal well near Youngstown, OH raised concerns of possible injection-induced seismicity. ODNR and Lamont–Doherty Earth Observatory (LDEO) deployed a local seismic network in December 2011 that more closely constrained the proximity of events to the injection well. Injection activities were ceased on 30 December 2011. On 31 December 2011, a M 4.0 earthquake occurred with an epicenter less than 1 km from the well. Several subsequent studies of this sequence have provided additional evidence that the earthquakes were induced by wastewater injection (ODNR, 2012; Kim, 2013; Holtkamp et al., 2013). Although uncommon, this finding is consistent with earlier cases where injection of fluids into underground formations have induced earthquakes (e.g., Evans et al., 2012; McGarr et al., 2002; Nicholson and Wesson, 1990). However, earthquakes caused by injection have become an important topic, as the use of multi-stage, hydraulic-fracturing well completions, which produce large volumes of wastewater, have become more commonplace in the oil and gas industry (e.g., NAS, 2012).

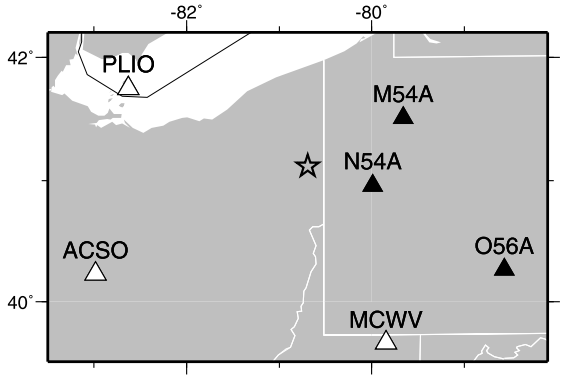

Fig. 1. Map of the Youngstown, OH (star) region showing seismic stations locations, with all triangles used for double difference relocation and black triangles used for template matching.

One of the key techniques utilized in previous studies of the Youngstown sequence is seismic waveform template matching, which involves cross-correlation of a set of seismograms from a known event with years of continuous data to detect similar signals. Template matching is known to lower the seismic event detection threshold by about 1.0 magnitude unit beyond what standard processing detects (e.g., Schaff, 2008; Schaff and Waldhauser, 2010). The method is well suited for studies of potentially induced seismicity that have multiple small earthquakes with similar

* Corresponding author.
E-mail addresses: skoumarj@miamioh.edu (R.J. Skoumal), brudzimr@miamioh.edu (M.R. Brudzinski), curriebs@miamioh.edu (B.S. Currie), levyj@miamioh.edu (J. Levy).
[1] Tel.: +1 515 401 8271.
[2] Tel.: +1 513 529 3216.

http://dx.doi.org/10.1016/j.epsl.2014.08.033
0012-821X/

waveforms because they are located within about a quarter wavelength of each other. Previous studies of the Youngstown sequence were able to identify ~100–300 events with this approach (Kim, 2013; Holtkamp et al., 2013), but neither sought to optimize the technique to identify as many events as possible. Moreover, a more flexible tool is needed for the broader application of analyzing the significant increase in potentially induced earthquakes (Ellsworth, 2013).

Within the central and eastern United States, the earthquake count has increased dramatically over the past few years. More than 300 earthquakes with $M \geq 3$ occurred in the 3 years from 2010 through 2012, compared with an average rate of 21 events/year observed from 1967 to 2000. Arkansas, Colorado, New Mexico, Ohio, Oklahoma, and Texas have recently experienced elevated levels of seismic activity near industrial activities, suggesting that these events were induced by human activity (e.g., Frohlich, 2012; Horton, 2012; Kerenan et al., 2013; Kim, 2013; Rubinstein and Ellsworth, 2013). With an optimized template-matching tool, tens of millions of template correlations can be performed every second allowing better characterization of seismic sequences. The advent of IRIS Web Services facilitates the versatility of this tool, allowing datasets in new regions of interest to be scanned without requiring large amounts of locally available storage space to host the large volumes of data.

This study builds on the previous work by Kim (2013) and Holtkamp et al. (2013) seeking to find the optimal template matching approach for the Youngstown earthquake sequence. In particular, Holtkamp et al. (2013) focused on correlating seismicity to injection operations while this paper focuses on improving the resolution of seismicity in space and time. We investigate variations in the seismic stations included, the total number of templates, the waveform passbands, the template seismogram lengths and start times, and the data request method. The optimized template matching approach is utilized to construct an expanded event catalog, including Richter scale magnitudes referenced to ODNR-reported events, which provides new opportunities to investigate the Gutenberg–Richter relationship and possible remote triggering. We use the multi-station cross-correlation matrix to perform double difference relocation on the expanded catalog. Ultimately, we intend the optimization procedure described here to help guide future efforts to investigate the growing number of potentially induced earthquakes.

2. Data and analysis

2.1. Cross-correlation and processing procedure

The cross-correlation coefficients (CCC) were calculated by cross-correlating the template through all available waveforms shifting one datum at a time. The sum of the normalized CCC values across the network for each time step was divided by the number of stations contributing to the sum, producing the network normalized CCC values (NNCCC). The daily median absolute deviation (MAD) of the NNCCC multiplied by 15 was used as a threshold to limit the number of false positives. Since the MAD is the 75th percentile of a symmetric distribution with zero mean, we estimate that the $15 \times$ MAD threshold would result in ~1 false positive per year given the number of samples per year with a nominal 40 samples per second.

To determine the optimal template parameters, we constructed a wide range of templates based on seismic arrivals from the first well-recorded and reported earthquake on 17 March 2011. We focused our template evaluations on correlations made during a month long time frame in March 2011, which encompassed a couple weeks before and after the template earthquake. The optimal target template sought is one that maximizes the number of detections that visually resemble the earthquake template while minimizes the number of false positives that have no visible hint of the earthquake template waveform features.

In this process, we considered over 30 station combinations from the Ohio Seismic Network and the Transportable Array, and we found the optimal station combination to be Transportable Array stations N54A, M54A, and 056A. We investigated a variety of bandpass filter ranges, with a lower limit typically between 1 and 5 Hz and upper limit between 10 and 20 Hz (limited by the sample rate at most stations). We found the optimal bandpass filter for this region to be 5–15 Hz. We also tested a wide variety of template durations for each station waveform from 5 to 60 seconds. Our results indicated that a template length of 37 s is an optimal choice for minimizing false positives and negatives, longer than the 20 s template length used by Holtkamp et al. (2013). Our study also compared templates where the start time of those windows is 10 s before the S wave arrival time on all channels with templates where the start time is 10 s before the P-wave arrival time on the vertical channel and 10 s before the S-wave arrival time on the horizontal channels. We found the latter to be slightly more effective.

2.2. Matched earthquake source locations and magnitudes

Template matching facilitates making a cross-correlation matrix between matched events that can serve as a powerful resource for obtaining precise relative arrival times that can be utilized for determining relative source locations of matched earthquakes. Our approach was to first manually pick the P and S arrival times on all stations with clear records (N54A, M54A, O56A, MCWV, ACSO, PLIO) for the 10 template events. We then used the correlation lag times between the template and each matched event to make appropriate pick times for each matched event assuming they have the same source properties. For events that match with more than one template, we used the template with the highest CCC. The arrival times for each event were used in an efficient absolute earthquake location routine (elocate Hermann, 2004) to serve as the "catalog" location for each matched event. Next, we used the full cross-correlation matrix between all events to establish precise relative P- and S-wave pick times between event pairs as input for double difference relocation.

We refined the event locations in a relative sense with the hypoDD double-difference algorithm (Waldhauser and Ellsworth, 2000; Waldhauser, 2001). The hypoDD algorithm iteratively solves for hypocentral variations, in a least-squares sense, by minimizing the residuals of travel-time differences between pairs of nearby events recorded on a common station, thus removing bias due to velocity model errors. The 1-D velocity model used for this processing follows that of Holtkamp et al. (2013) developed for the same purpose, but it differs somewhat from Kim (2013) as the stations we used are much farther from the source region (see Supplementary Material). Considering the deployment of Kim (2013) did not begin until late November 2011 and only lasted a couple months, our long-term analysis did not utilize the local data and thus had difficulties determining accurate absolute locations. We addressed this by using the hypocentral location of the 24 December 2011 earthquake from the local deployment of Kim (2013) as the absolute reference point and shifted all hypodd results by the difference between Kim's location and our hypodd location for this event (about 1 km). We determined relative location uncertainties using bootstrapping, removing one station at a time from the location process and using the standard deviation as the error estimate (Efron, 1979). We then restricted our analysis to focus on events with low relative location uncertainties and RMS arrival time misfits.

We determined local magnitudes through a simple Richter scale approach. For each station and component in our final templates, we calculated the median scale factor (Ao) using the S waveform amplitudes and catalog magnitudes for all 12 events reported by ODNR. For each matched event, we calculated a magnitude from the scale factor and S waveform amplitude at each station and component, and took the median value as our final magnitude.

3. Results

3.1. Template matching

We found the optimal template to be three EarthScope USArray stations (N54A, M54A, O56A), such that our results are based on scanning templates from the inception of recording in November 2010 to the end of this study in February 2014. Although increasing the number of template earthquakes produced a similar diminishing return in number of matched events to that seen in Holtkamp et al. (2013), we decided to utilize all 12 ODNR detected events as templates. The correlation procedure found 566 unique events once the template results were merged and duplicate matches from different templates were discarded. On average, each template found 236 events, while the earliest template found as many as 337 events, and the results of each were combined to form a single catalog of unique events. The earliest matched event occurred on 11 January 2011, 13 days after sustained injection began. Remarkably, our technique found 56 matched events before the first ODNR reported earthquake (M 2.1, 17 March 2011) in the series. Waveforms showing the waveform similarity for the first 56 matched earthquakes is provided in the Supplementary Material (Fig. S1a). Nearly all of these events were matched by the first ODNR reported earthquake template (54 of 56). This result underscores the importance of optimizing the template matching procedure such that it can be run in real-time when new events are recorded in the central and eastern US to help determine if a reported earthquake is part of a growing sequence or an isolated event.

As in Holtkamp et al. (2013), the number of earthquakes over time closely followed the injection history (Fig. 2), with a gradual rate increase at the beginning of the sequence and an abrupt reduction in earthquake rate after injection ceased. As described in several previous studies of injection related seismicity (NAS, 2012; Ellsworth, 2013; Kim, 2013; Holtkamp et al., 2013), we interpret that the fluids injected into Precambrian crystalline rocks at the base of the injection interval reduced the effective normal stress on pre-existing faults or fractures with orientations optimal to initiate slip, given the orientation of the regional maximum horizontal stress field in the Youngstown area (~050°) (Zoback, 1992).

Our catalog is consistent with the four phases defined by Holtkamp et al. (2013) based on injection history, seismicity rate, earthquake magnitudes, and waveform similarity (Figs. 2 and S1). The initial phase began soon after the initiation of commercial injection operations (28 December 2010), the second phase began soon after injection pressures are approved to exceed 2500 psi (3 May 2011), and the third phase began soon after sustained daily injection volumes in excess of 2000 BBL (3 August 2011), ending 2 weeks after injection ended. We referred to all earthquakes more than 2 weeks after shut in as phase four, noting that earthquakes originating at some distance from the injection point will not respond to shut in until the pore pressure "back front" (analogous to the pore pressure triggering front), arrives some discrete time later (Shapiro and Dinske, 2009). The waveform shapes of the best matched events in our catalog help illustrate the main phases of the sequence (Fig. S1b), although there are several events at the beginning of phase three that were more similar to those in phase two. We inferred that the waveforms changed shape as the source moved to new locations over time, as analyzed in Section 3.2.

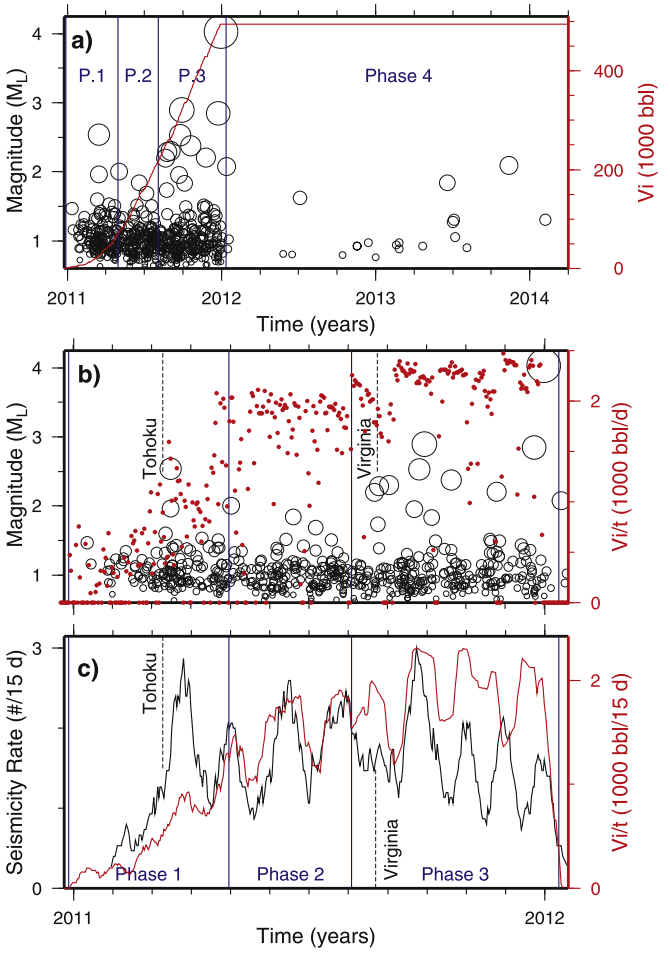

Fig. 2. Comparison of matched earthquakes with volumes of injected wastewater (Vi). Blue lines divide phases of the injection and earthquake sequence as defined by Holtkamp et al. (2013). Dashed lines mark times of remote earthquakes that produced large surface waves in the Youngstown area. (a) Magnitudes of all matched events over time (circles), compared with cumulative injection volume (red). (b) Earthquake magnitudes (circles) and daily injected volume (Vi/t, red dots) during the period of injection. (c) Seismicity rate (black) and injection rate (red) in the preceding 15 days, plotted for each day during the injection. (For interpretation of the references to color in this figure, the reader is referred to the web version of this article.)

We note that the magnitude distribution of larger earthquakes during the different phases remains consistent with earlier studies, but our catalog provides more information regarding the lower end of the magnitude scale. To help characterize the magnitude distribution, we investigated the b-values obtained from the Gutenberg–Richter relationship between seismicity amounts and magnitudes. In most cases, b-values are expected to be ~1 as scale-invariant relationships are common in nature, but seismicity associated with fluid injection often have b-values <1 (Lei et al., 2008; Bachmann et al., 2014), with the lowest b-values often observed during the largest injection rates. Fig. 3a shows the magnitude–occurrence relationships for our catalog, with the roll-off indicating our magnitude of completeness is approximately 0.9. Using events at this magnitude and above, we linearly fit the events resulting in a b-value of 0.82, which is consistent with previous studies of potentially induced seismicity with b-values less than 1. However, the relationship is clearly not linear with an apparent high b-value for lower magnitudes and a lower b-value for higher magnitudes. When we separated the catalog into the four phases (Fig. 3b–e), the b-values are 1.33, 1.92, 0.67, and 0.73. During phases 1 and 2, more events smaller than M 1.5 occurred than expected during periods of normal seismicity. During phase 3, a similar relationship

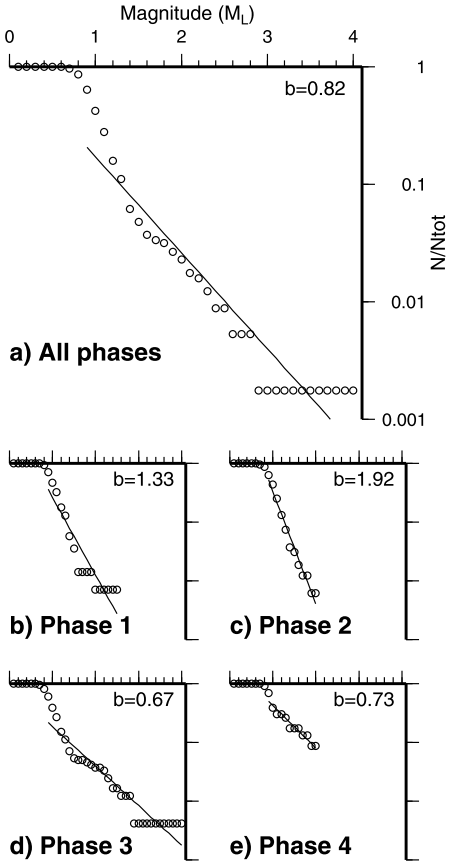

Fig. 3. Magnitude–occurrence relationships for (a) all matched events and (b–e) separate phases of the sequence. N/N_{tot} is the number of events at or above a given magnitude divided by the total number of events. b indicates the Gutenberg–Richter b-value for the distribution, where 1 is commonly observed for natural seismicity.

can be identified in these small events in addition to a large number of M 2+ events. After injection had ceased during phase 4, only events less than M 2 were recorded, albeit at a very similar b-value identified in phase 3.

The identified b-values during each phase are similar to some aspects of previous induced seismicity studies on fluid injection. Phases 1 and 2 in Youngstown demonstrate an increasing b-value (Fig. 3) and event rate (Fig. 2) that is not a common feature of induced seismicity, but this trend has been observed in China and Switzerland during early stages of injection marked by lower but increasing injection rate and fluid pressure (Lei et al., 2013; Bachmann et al., 2012). While the increase is uncommon, we note that our maximum b-values in phase 2 are near to 2.0, a value reported for hydraulic fracturing (Maxwell et al., 2009; Wessels et al., 2011) suggesting this may have occurred during this phase in Youngstown. Our phase 3 shows a period of high injection rate, high event rate, and low but variable b-value (Figs. 2 and 3), which is similar to later stages of injection for the two cases in China (Lei et al., 2008, 2013). Our phase 4 corresponds to the period after injection, marked by a low seismicity rate and small b value, also seen in several previous cases.

3.2. Double difference relocation

Our initial estimates of the hypocenters for all of our matched events utilizing P and S times based on correlations to the best matching template are shown in Fig. 4a. The cloud of seismicity has a radius of ~5 km, but there is some clustering in an east–west oriented rectangle that is 3–4 km long in the center of the cloud. Application of double difference relocation refined the dataset, initially discarding 110 airquakes with large uncertainties. We further limited the results by focusing on events that had relative location uncertainties less than 10 m horizontally and 60 m vertically and RMS residuals less than 0.35 s for catalog and cross-correlation data. Fig. 4b shows that the remaining 140 events that meet this criteria, which define a linear streak extending from near the well to ~800 m WSW with a strike of 258°. However, if we examine the seismicity closely, we find that the distribution indicates a set of en echelon faults as suggested by Kim (2013) based on fewer events. The strike of these smaller faults are 263°, closer to that of the fault plane solution (265°), and consistent with the regional stress field and well basement fracture orientation (Kim, 2013; Holtkamp et al., 2013). A cross-sectional view of our relocated hypocenters shows the depths are focused in the Precambrian basement in the 3.5–4.0 km range (Fig. 5), consistent with those of Kim (2013). While the events form a nearly vertical feature, our relocated events show a ~88° dip to the north that is slightly different than the fault plane solution dip of 72° to the north. Nevertheless, the hypocentral distribution, correlated waveforms, and determined focal mechanism indicate that many if not all events in the sequence are a series of left-lateral slips along a near vertical east–west oriented basement fault (or faults).

Events early in the sequence were located very close to the Northstar 1 injection well (<100 m) and then gradually extend further away over time (Fig. 4). Fig. 6 shows the distances away from the well of the 140 best relocated epicenters over time. The symbol size in Fig. 6 shows the approximate average horizontal location uncertainty using the y-axis for scale. A simple line fit to the relocated events indicates a migration velocity (v) of 1.0 m/d, but this line does not intersect the well at time zero (when sustained injection began on 22 December 2010), suggesting that this approximation is not appropriate. Based on work in previous induced seismicity studies, we considered a propagation rate approximation by considering a point source of pore pressure perturbation from the injection. In an infinite, hydraulically homogeneous, and isotropic fluid-saturated medium, the triggering front $r(t)$ has the following form (Shapiro et al., 1997):

$$r(t) = \sqrt{4\pi Dt}$$

where t is the time from the injection start and D is the hydraulic diffusivity. Using the apparent migration front defined by the best located seismicity (black dots, Fig. 6), we searched for the optimal D value to minimize the difference between the apparent front and the predicted r. The best fitting diffusivity was 0.0017 m^2/s but the constant diffusivity does a poor job of fitting the shape of the migration front over time (residual sum of squares, RSS = 0.126).

In October 2011, 74 m of sediment fill-up was identified in the Northstar 1 injection well (ODNR, 2012). To account for the sediment clogging of the fault, we suggest that the rate of sediment fill-up is proportional to the rate of injection which, in turn, is proportional to the diffusivity. Therefore, the rate of change of the diffusivity is proportional to the diffusivity:

$$\frac{dD}{dt} = -kD$$

The diffusivity can then be expressed as an exponential function with time:

$$D = ae^{-kt} + b$$

where:

$$D_0 = a + b$$

$$D_\infty = b$$

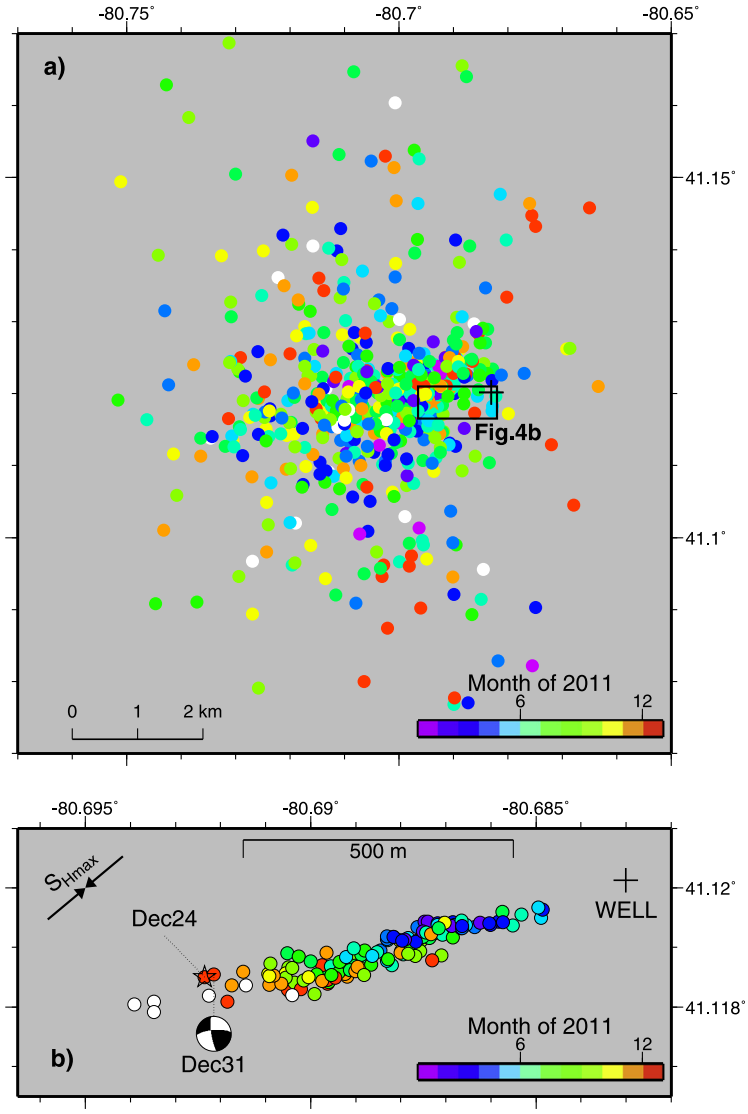

Fig. 4. Map of epicenters determined from our analysis, colored by month of 2011 (white indicates 2012–2014). Cross indicates Northstar #1 injection well. (a) Epicenters determined using P and S times based on correlations to the best matching template. (b) Double-difference relocated hypocenters using a full matrix of cross-correlations for all events. Only events with low location uncertainty and RMS error are plotted. Absolute locations are based on the 24 Dec. 2011 earthquake (star) located with local data (Kim, 2013). Focal mechanism is from the 31 Dec. 2011 M 4 earthquake (Kim, 2013). Arrows show maximum compressive stress orientation (S_{Hmax}) (Mazzotti and Townend, 2010). (For interpretation of the references to color in this figure, the reader is referred to the web version of this article.)

Considering that injection of large volumes continued until shut-in, the constant (b) is necessary to avoid the diffusivity function going to 0 m^2/s. A grid-search approach was used to find the optimal values of a, b, and k to minimize the misfit between the migration front and the predicted r (Fig. 6). This estimate of the diffusivity that approximates the clogging of the well provides a better fit to our observations (RSS = 0.003). Accounting for the different degrees of freedom for the two diffusivity models, an f-test indicates the decaying D model is a significantly better representation of the data at a 99.99% confidence level.

3.3. Earthquake triggering

A recent study found several areas in the Midwestern US with suspected induced seismicity are also more susceptible to earthquake-triggering from natural transient stresses generated by the seismic waves of large remote earthquakes (van der Elst et al., 2013). This study concluded that enhanced triggering susceptibility suggests the presence of critically loaded faults and potentially high fluid pressures. However, they found that triggering of Youngstown seismicity from the surface waves of the 7 April 2011 M 9.0 Tohoku earthquake was inconclusive. Since their study only used a single station to do template matching, our catalog of Youngstown seismicity is more extensive and can better examine seismicity rates over time (Fig. 2). Our catalog has 10 events in the 10 days before the Tohoku event and 24 events in the 10 days after the Tohoku earthquake (Fig. 7a), similar to other cases of triggered seismicity (van der Elst et al., 2013). However, there was also an increase in the daily injected volumes after the Tohoku earthquake that followed a similar trend to the increase in seismicity during this time. This is consistent with earlier work on the Youngstown earthquake sequence that found that cumulative seismicity was proportional to cumulative injected volume (Holtkamp et al., 2013). The seismicity rate over 15 day time periods using our catalog also correlates with the injection rate (Fig. 3c), but there is a larger than expected increase in seismicity rate in the 15 days after the Tohoku event, suggesting that some portion of the increased seismicity may have been remotely triggered by this event.

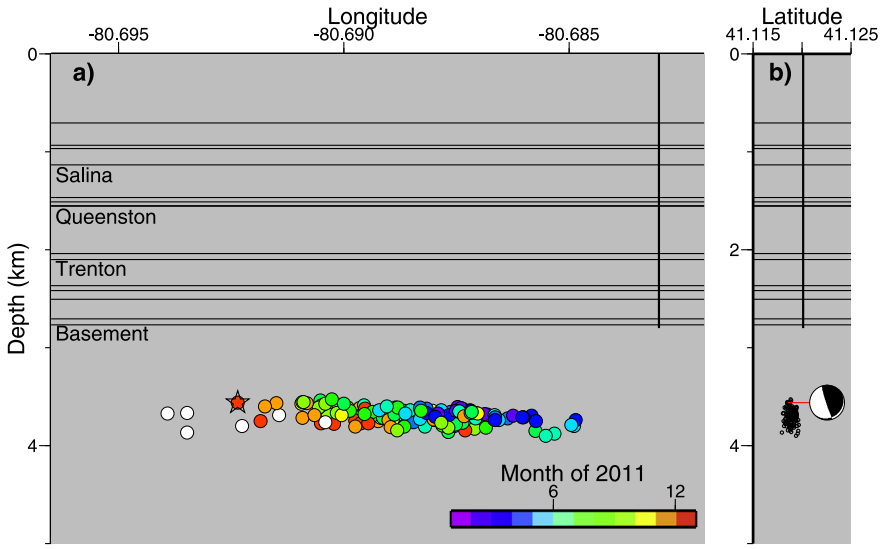

Fig. 5. East–west (a) and north–south (b) cross-sections of the double-difference relocated seismicity. Absolute depths are based on the Dec. 24, 2011 earthquake (star) located with local data (Kim, 2013), placing the events within the Precambrian basement. Horizontal lines mark key strata and the vertical line is the Northstar 1 injection well. Back hemisphere projection of the focal mechanism for the 31 Dec. 2011 M 4 earthquake shows a similar near-vertical dip between the fault plane and the seismicity. Horizontal exaggeration is 6.5× in (a), no exaggeration in (b).

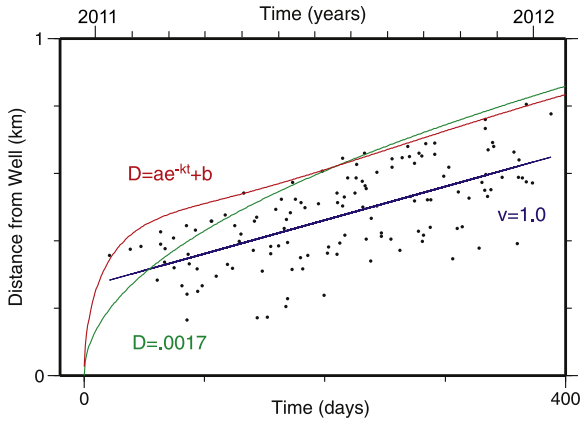

Fig. 6. Estimation of fluid diffusion based on earthquake migration. Distance of relocated epicenters (dots) from the injection well over time. We use the events with the smallest uncertainties to investigate potential fluid diffusion. Diffusion curves that include the decaying diffusivity due to sediment fill up (red) match the migration front better than those with a constant diffusion (green). Blue line indicates best fitting linear migration velocity (v), although a physical basis for this is unclear since it does not intersect the well location. (For interpretation of the references to color in this figure, the reader is referred to the web version of this article.)

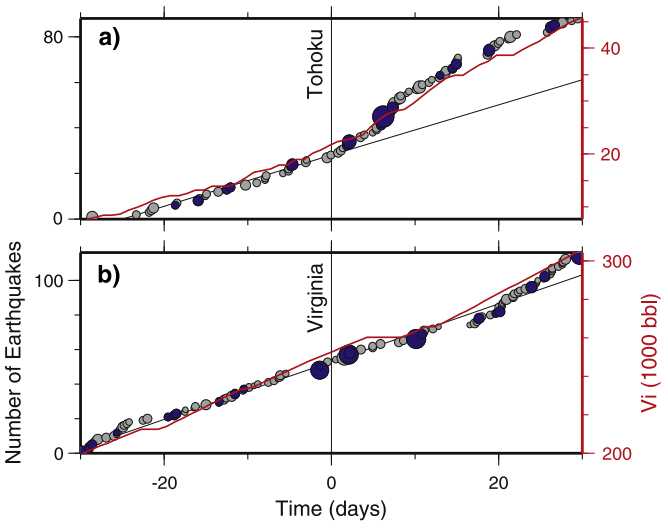

Fig. 7. Examination of the enhanced Youngstown earthquake catalog for evidence of triggering due to remote earthquakes similar to the study of van der Elst et al. (2013). Cumulative number of earthquakes (circles) and injected volume (red) are shown around the (a) M 9.0 Tohoku earthquake on 7 April 2011 and (b) M 5.8 Virginia earthquake on 23 August 2011. Well located events from Fig. 4b are highlighted in blue. (For interpretation of the references to color in this figure, the reader is referred to the web version of this article.)

We also checked for a triggering trend associated with the 23 August 2011 M 5.8 Virginia earthquake but found no significant increase in earthquake numbers in the 10 days following that event (Fig. 7b). There appears to be a slight increase in seismicity ~20 days after the event, but this is commensurate with an increase in injected volume and rate. We note that there are several larger ($M > 2$) earthquakes following the Virginia event (Fig. 3a), but this trend begins just before the potential trigger occurs (Fig. 7b). The lack of prominent triggering suggests this process is not linearly related to seismic wave displacement considering the surface wave displacements are a factor of 5 larger than the Tohoku event when they reach the Youngstown area. The largest earthquake to occur after injection stopped was the 11 April 2012 Indian Ocean earthquake sequence (M 8.6 and 8.2). While not quite as large as the Tohoku event, we found no matched events within 30 days of 11 April 2012. Therefore, it does not appear that triggering occurred after injection stopped.

4. Conclusions

Creating an optimized correlation procedure was important to provide a more detailed study of the Youngstown sequence that can also be applied to study the large increase in earthquake activity in the U.S. midcontinent identified by Ellsworth (2013). The ideal template matching parameters for the Youngstown sequence were determined by modifying the stations used, bandpass filter range, template length, and template start time. The resulting catalog from this routine was consistent with the sequence determined by Holtkamp et al. (2013), while also identifying hundreds of additional events. The hypoDD results located the start of Youngstown sequence within 100 m of the Northstar 1 injection well which then gradually extended 500 m westward during 2011. We suggest that the earthquake migration front, which was observed to

have a similar trend to the daily average injection pressures, could be influenced by decaying diffusivity over time, possibly caused by clogging due to injection. A b-value of < 1 was observed for the entire sequence, consistent with other fluid induced seismicity studies. We also note that the abnormally high b-value of 1.92 during phase 2 is comparable to b-values obtained during hydraulic fracturing.

Acknowledgements

Support for this work was provided by NSF grant EAR-0847688 (M.B.). This works builds directly on that of Steve Holtkamp so we are grateful for all of his advising in putting this study together. We benefited from discussions with Danielle Sumy, Chad Trabant, Heather DeShon, Chris Grope, and many folks at the Ohio Geological Survey. The manuscript was improved based on constructive reviews by editor Peter Shearer and 2 anonymous reviewers.

Appendix A. Supplementary material

Supplementary material related to this article can be found online at http://dx.doi.org/10.1016/j.epsl.2014.08.033.

References

Bachmann, C.E., Wiemer, S., Goertz-Allmann, B.P., Woessner, J., 2012. Influence of pore-pressure on the event-size distribution of induced earthquakes. Geophys. Res. Lett. 39, L09302. http://dx.doi.org/10.1029/2012GL051480.

Bachmann, C.E., Foxall, W., Daley, T., 2014. Comparing induced seismicity on different scales. In: Proceedings, Thirty-Ninth Workshop on Geothermal Reservoir Engineering. Stanford University, Stanford, CA.

Efron, B., 1979. Bootstrap methods: another look at the jackknife. Ann. Stat. 7 (1), 1–26. http://dx.doi.org/10.1214/aos/1176344552.

Ellsworth, W.L., 2013. Injection-induced earthquakes. Science 341. http://dx.doi.org/10.1126/science.1225942.

Evans, K.F., Zappone, A., Kraft, T., Deichmann, N., Moia, F., 2012. A survey of the induced seismic responses to fluid injection in geothermal and CO_2 reservoirs in Europe. Geothermics 41, 30–54. http://dx.doi.org/10.1016/j.geothermics.2011.08.002.

Frohlich, C., 2012. Two-year survey comparing earthquake activity and injection-well locations in the Barnett Shale, Texas. Proc. Natl. Acad. Sci. USA 109, 13934–13938. http://dx.doi.org/10.1073/pnas.1207728109.

Hermann, R.-B., 2004. Computer programs in seismology, Version 3.30-GSAC.

Holtkamp, S., Currie, B., Brudzinski, M., 2013. A more complete catalog of the 2011 Youngstown, Ohio earthquake sequence from template matching reveals a strong correlation to pumping at a wastewater injection well. AAPG Search and Discovery Article #90163. 2013 Annual Convention and Exhibition, Pittsburgh, May 19–22.

Horton, S., 2012. Disposal of hydrofracking waste fluid by injection into subsurface aquifers triggers earthquake swarm in central Arkansas with potential for damaging earthquake. Seismol. Res. Lett. 83, 250–260. http://dx.doi.org/10.1785/gssrl.83.2.250.

Kerenan, K.M., Savage, H.M., Abers, G.A., Cochran, E.S., 2013. Potentially induced earthquakes in Oklahoma, USA: links between wastewater injection and the 2011 Mw 5.7 earthquake sequence. Geology 41, 699–702. http://dx.doi.org/10.1130/G34045.1.

Kim, W.-Y., 2013. Induced seismicity associated with fluid injection into a deep well in Youngstown, Ohio. J. Geophys. Res. 118, 3506–3518. http://dx.doi.org/10.1002/jgrb.50247.

Lei, X., Yu, G., Ma, S., Wen, X., Wang, Q., 2008. Earthquakes induced by water injection at ~3 km depth within the Rongchang gas field, Chongqing, China. J. Geophys. Res. 113, B10. http://dx.doi.org/10.1029/2008JB005604.

Lei, X., Ma, S., Chen, W., Pang, C., Zeng, J., Jiang, B., 2013. A detailed view of the injection-induced seismicity in a natural gas reservoir in Zigong, southwestern Sichuan Basin, China. J. Geophys. Res. 118, 1–16. http://dx.doi.org/10.1002/jgrb.50310.

Maxwell, S.C., Jones, M., Parker, R., Miong, S., Leaney, S., Dorval, D., D'Amico, D., Logel, J., Anderson, E., Hammermaster, K., 2009. Fault activation during hydraulic fracturing. In: SEG Annual Meeting, Expanded Abstracts.

Mazzotti, S., Townend, J., 2010. State of stress in central and eastern North American seismic zones. Lithosphere 2 (2), 76–83. http://dx.doi.org/10.1130/L65.1.

McGarr, A., Simpson, D., Seeber, L., 2002. Case histories of induced and triggered seismicity. In: Lee, W., Kanamori, H., Jennings, P., Kisslinger, C. (Eds.), International Handbook of Earthquake and Engineering Seismology, vol. 40. Academic Press, London, pp. 647–664.

National Academy of Sciences (NAS), 2012. Induced Seismicity Potential in Energy Technologies. Natl. Acad. Press, Washington, DC. 225 pp.

Nicholson, C., Wesson, R.L., 1990. Earthquake hazard associated with deep well injection: a report to the U.S. Environmental Protection Agency. U.S. Geol. Surv. Bull. 1951. http://pubs.usgs.gov/bul/1951/report.pdf.

Ohio Department of Natural Resources (ODNR) (2012). Preliminary report on the Northstar 1 class II injection well and the seismic events in the Youngstown, Columbus, Ohio. 23 pp.

Rubinstein, J.L., Ellsworth, W.L., 2013. The 2001–present triggered seismicity sequence in the Raton basin of southern Colorado/northern New Mexico. Seismol. Res. Lett. 84, 374.

Schaff, D.P., 2008. Semiempirical statistics of correlation-detector performance. Bull. Seismol. Soc. Am. 98, 1495–1507. http://dx.doi.org/10.1785/0120060263.

Schaff, D.P., Waldhauser, F., 2010. One magnitude unit reduction in detection threshold by cross correlation applied to Parkfield (California) and China seismicity. Bull. Seismol. Soc. Am. 100, 3224–3238. http://dx.doi.org/10.1785/0120100042.

Shapiro, S.A., Dinske, C., 2009. Fluid-induced seismicity: pressure diffusion and hydraulic fracturing. Geophys. Prospect. 57, 301–310. http://dx.doi.org/10.1111/j.1365-2478.2008.00770.x.

Shapiro, S.A., Huenges, E., Borm, G., 1997. Estimating the crust permeability from fluid-injection-induced seismic emission at the KTB site. Geophys. J. Int. 131, F15–F18. http://dx.doi.org/10.1111/j.1365-246X.1997.tb01215.x.

van der Elst, N.J., Savage, H.M., Keranen, K.M., Abers, G.A., 2013. Enhanced remote earthquake triggering at fluid-injection sites in the midwestern United States. Science 341, 164–167. http://dx.doi.org/10.1126/science.1238948.

Waldhauser, F., 2001. Hypodd: a computer program to compute double-difference earthquake locations. USGS Open File Rep. 01-113, http://pubs.usgs.gov/of/2001/0113/pdf/hypoDD.pdf.

Waldhauser, F., Ellsworth, W.L., 2000. A double-difference earthquake location algorithm: method and application to the northern Hayward fault, California. Bull. Seismol. Soc. Am. 90, 1353–1368.

Wessels, S., Kratz, M., De La Pena, A., 2011. Identifying fault activation during hydraulic stimulation in the Barnett shale: source mechanisms, b values, and energy release analyses of microseismicity. In: SEG Annual Meeting, Expanded Abstracts.

Zoback, M. Lou, 1992. Stress field constraints on intraplate seismicity in Eastern North America. J. Geophys. Res., Solid Earth 97 (B8), 11761–11782.